Communication

Rotated Feed-Combined Reconfigurable Transmit RIS With Disparate Deployment of 1-bit Hybrid Units for B5G/6G

Jaehoon Kim, Jinhyun Kim, Jun Hwa Oh, Sang-Hyuk Wi, and Jungsuek Oh

***Abstract*— This communication presents an initial disparate deployment of 1-bit hybrid units using p-i-n diodes in transmit reconfigurable intelligent surface (TRIS) combined with a rotated feed source to address the gain limitation of the existing 1-bit TRIS. Two types of hybrid units, with a radiation phase difference of 90° by the delay line, are proposed in this study. The TRIS aperture is divided into two sections based on two different radiation centers by rotated feed, and the hybrid units in each section are initially configured to implement optimized quasi 2-bit beam collimation in the 0° and 40° for enhanced quantization loss. It is found that the array envelope is higher even in radiation directions other than the optimized directions, despite the initial disparate deployment of each section. Beamforming for −theta direction in the H-plane is only considered for the proof of concept with the smallest size of TRIS aperture. A 16 × 16 (7.6 × 7.6 λ_0 at 28 GHz) 1-bit hybrid TRIS offers gain enhancement of 0–5.6 dB in −70° to −0° directions of the array envelope compared with the conventional 1-bit TRIS. The proposed 1-bit hybrid TRIS yields an improved aperture efficiency of 24.4%.**

***Index Terms*— Array envelope, beamforming, hybrid, p-i-n diodes, quantization, transmit reconfigurable intelligent surface (TRIS).**

I. Introduction

The era of 5G has arrived with the commercialization of mmWave in response to consumer demand for high-speed and low-latency communication. As a result, several studies have focused on high-gain antennas operating in low-loss systems to improve communication capacity since the mmWave band has critically degraded RF path loss. The development of an electronically reconfigurable antenna that can dramatically reduce the lossy components in the RF integrated circuit (RFIC) is attracting attention due to the inherent characteristics of the RF system, in which the insertion loss increases rapidly as the frequency increases [1]. In particular, reconfigurable intelligent surface (RIS) operating as a spatial beamformer is considered a promising beamforming solution since it can eliminate the beamforming IC and implement beam steering by using a low-loss dc control circuit [2], [3], [4], [5], [6], [7]. Liquid crystal, varactor diode, and p-i-n diode are typically used as reconfigurable components constituting an electrically controllable unit cell. In contrast to liquid crystals, p-i-n diodes can enable the implementation of beam switching at the nanosec level, in which high-speed switching is limited by the reorganization speed of molecular arrangement. In addition, the p-i-n diode has a relatively high Q-factor at high frequency compared to the varactor diode, which makes it suitable for realizing a low-loss unit cell. Most reconfigurable unit cells based on p-i-n diodes employ the 1-bit current inversion method [8], [9]. Although this has the advantage of implementing a compact unit cell topology, it exhibits large gain degradation due to the fundamental limitation of 1-bit quantization loss [11]. Clemente et al. [2] presented a numerical analysis of p-i-n diode-based transmit reconfigurable intelligent surface (TRIS) successfully but reported high quantization loss of 4 dB. Diaby et al. [3] tried to improve the quantization loss by employing a 2-bit unit cell, but only reported an aperture efficiency of 15.9%. Wang et al. [5] reported a relatively high aperture efficiency of 22.6% by using asymmetric dipole elements. However, the implementation of a large area is limited since four bias lines are required per unit cell. Wang et al. [6] reported improved scan loss by using an equivalent magnetic dipole element but cannot overcome low broadside gain. Wang et al. [7] designed a subwavelength unit cell to enhance the stability of oblique incidence but eventually reported a low aperture efficiency of 14%.

Therefore, in this communication, we propose an initial disparate deployment of 1-bit hybrid units combined with a rotated feed source to overcome the low aperture efficiency of conventional 1-bit TRIS based on p-i-n diodes. Two types of 1-bit hybrid units with a radiation phase difference of 90° are arranged disparately in two sections according to the radiation centers of rotated feed

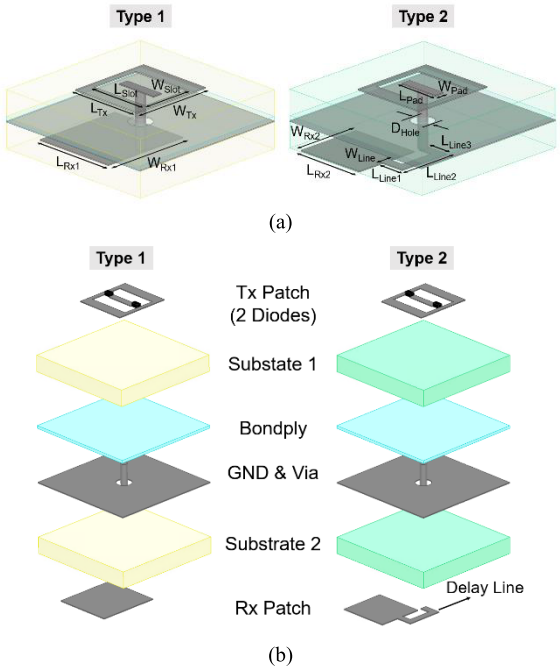

Fig. 1. (a) 1-bit hybrid units including design parameters and (b) its exploded view.

Manuscript received 4 August 2022; revised 18 January 2023; accepted 10 February 2023. Date of publication 28 February 2023; date of current version 2 June 2023. This work was supported by SAMSUNG Research, Samsung Electronics Co., Ltd. *(Corresponding author: Jungsuek Oh.)*

Jaehoon Kim, Jinhyun Kim, and Jungsuek Oh are with the School of Electrical and Computer Engineering, Institute of New Media Communication (INMC), Seoul National University, Seoul 152742, South Korea (e-mail: jaehoonkim@snu.ac.kr; jinhyun111@snu.ac.kr; jungsuek@snu.ac.kr).

Jun Hwa Oh and Sang-Hyuk Wi are with Samsung Research, Seoul 06765, South Korea (e-mail: james33.oh@samsung.com; sang-hyuk.wi@samsung.com).

Color versions of one or more figures in this communication are available at https://doi.org/10.1109/TAP.2023.3248374.

Digital Object Identifier 10.1109/TAP.2023.3248374

TABLE I
DESIGN PARAMETERS AND THEIR VALUES OF 1 BIT HYBRID UNITS IN FIG. 1

Parameters & Values					
L_{Rx1}	2.6	L_{Rx2}	2.25	L_{Line2}	1.7
W_{Rx1}	2.85	W_{Rx2}	2.1	L_{Line3}	0.75
L_{Tx}	2.35	L_{pad}	1.3	W_{Line}	0.3
W_{Tx}	2.6	W_{pad}	0.3		
L_{Slot}	1.95	D_{Hole}	0.7		
W_{Slot}	1.6	L_{Line1}	0.75		

(Unit : mm)

and operate as quasi 2-bit for improved array envelope. This quasi 2-bit beamforming demonstrates improved array envelope compared to conventional 1 bit one despite the disparate deployment. The configuration, operating principle, and transmit characteristics of 1-bit hybrid units by incident angle are presented in Section II. Then, the initial deployment of 1-bit hybrid units according to the radiation center of the rotated feed source is discussed. In Section III, simulation and measurement results are presented. Finally, Section IV concludes this communication.

II. DESIGN OF 1-BIT HYBRID TRIS

A. Hybrid Unit Cell Design

Fig. 1 shows the drawings of 1-bit hybrid units, including design parameters and an exploded view. The values of design parameters are shown in Table I. The Rx layer is composed of a square patch and the Tx layer is composed of a U-slot patch based on two p-i-n diodes. The Tx and Rx layers are connected by metallic via through GND layer. A delay line extending from the type 2 Rx patch creates a 90° phase difference between the two hybrid units. The two substrates are HF-350F from Taconic, with a thickness of 0.76 mm and a dielectric constant and loss tangent of 3.5 and 0.0029, respectively. The bondply is HB-360 from Taconic, with a thickness of 0.13 mm and a dielectric constant and loss tangent of 3.65 and 0.0032, respectively. The unit cell period is 5.1 mm (0.48 λ_0 at 28 GHz). Fig. 2(a) shows the unit cell configuration with asymmetrically mounted two p-i-n diodes and a compact dc bias topology. Two p-i-n diodes are mounted 87 asymmetrically between a rectangular ring and a center pad on the Tx layer. Therefore, the two diodes operate in different states by the dc voltage V_{DC} applied to the rectangular ring. A diode of the MADP-000907-14020 model is used, which operates as a series circuit of 5.2 Ω and 30 pH under positive bias and a parallel circuit of 0.025 pF and 30 pH under negative bias [10]. The center pad is in contact with the GND layer through the center via and the GND via. dc via is located at the middle point of the rectangular ring, which has the lowest electric field intensity for preventing RF leakage and is in contact with the dc line. Fig. 2(b) shows the surface current density of two types of hybrid units according to the state of two p-i-n diodes. The two diodes operate asymmetrically and realize a 180° phase difference by controlling the current distribution in each state. Two types of hybrid units have a 90° phase difference in the same state by the delay line in Fig. 1(b). Consequently, the two types of hybrid units have four transmission phases of an equally spaced 90° difference.

Fig. 3 shows the S21 and S21 phase of two 1-bit hybrid units with dc bias configuration according to the Floquet incident angle of the TE wave, as shown in Fig. 2(a). Two types of hybrid units have an insertion loss of less than 1 dB at 28 GHz in $\theta = 0°$ (normal incidence) condition. However, the insertion loss of type 2 with delay line increases to 2 dB in $\theta = 40°$ (steered incidence)

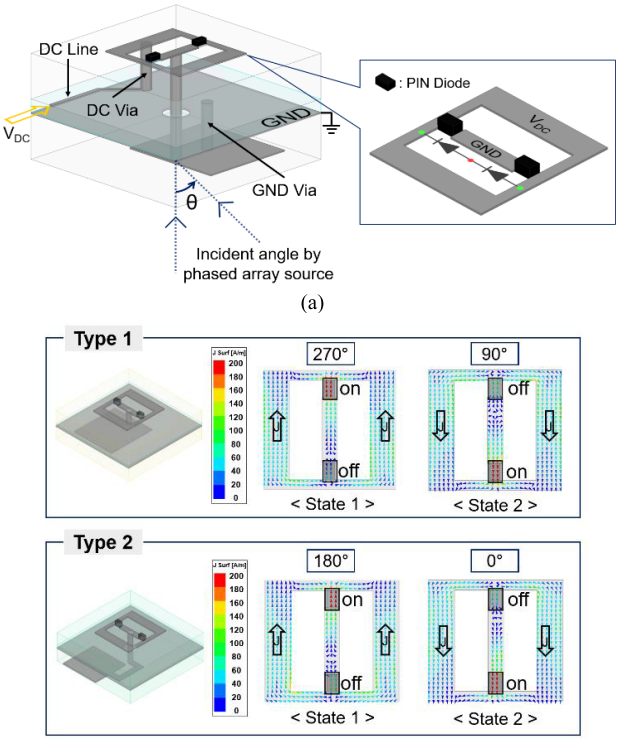

Fig. 2. (a) Unit cell with asymmetrically mounted two p-i-n diodes and compact dc bias configuration and (b) surface current density of two types of hybrid units according to the state of two p-i-n diodes.

TABLE II
EFFICIENCY OF THE 1 BIT HYBRID TRIS APERTURE ACCORDING TO THE ROTATED ANGLE OF FEED HORN

Angle of Horn	Spillover Efficiency	Illumination Efficiency	Total Efficiency
0°	0.69	0.73	0.51
40°	0.53	0.76	0.40

condition. In addition, type 2 deviates the transmission phase under the condition of $\theta = 40°$, which impairs the equally spaced four transmission phases. In conclusion, the type 2 with a delay line topology is sensitive to the incident angle and has deteriorated transmission characteristics with respect to insertion loss and phase when combined with a rotated feed source.

B. Deployment of 1 Bit Hybrid Units in Transmit RIS

Fig. 4(a) shows the rotated feed combined TRIS classified into two sections based on two different radiation centers by beam steering source. In this study, only two sections are employed to verify the unidirectional (−theta) beamforming cases. The TRIS aperture is shifted by 1.9 λ_0 from the feed center in the $-y$-direction to minimize the decrease in spillover efficiency due to the beam steering of the rotated feed source. The TRIS aperture is classified into two sections based on two different radiation centers by beam steering angle of $\theta = 0°$ and $\theta = 40°$. The focal length (F) based on Section I is 5 λ_0, and the aperture efficiency by the beam steering angle is calculated as Table II [12]. It should be noted that the total efficiency of TRIS with $\theta = 40°$ horn is 1 dB lower than that of TRIS with $\theta = 0°$ horn. Fig. 4(b) shows the electric field intensity of the TRIS aperture according to the rotated angle θ. The 1-bit hybrid units in Sections I and II can be deployed differently to have respective

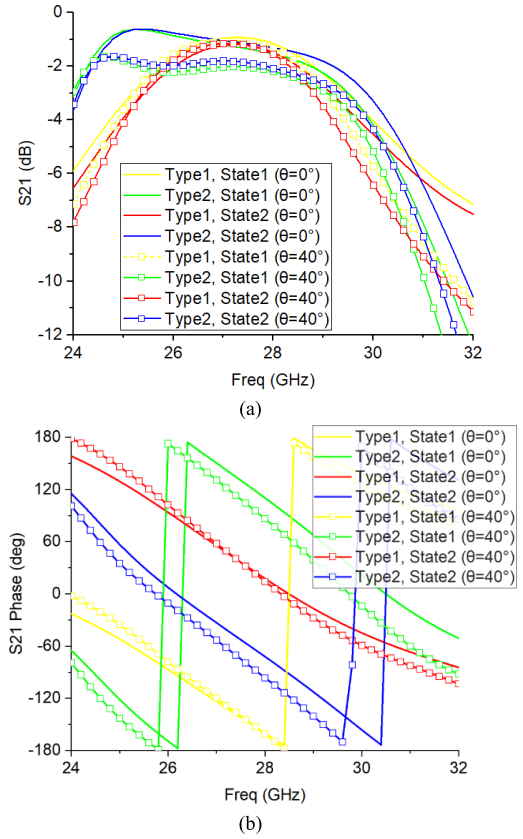

Fig. 3. (a) S21 and (b) S21 phase of two 1-bit hybrid units with dc bias configuration according to the Floquet incident angle of TE wave.

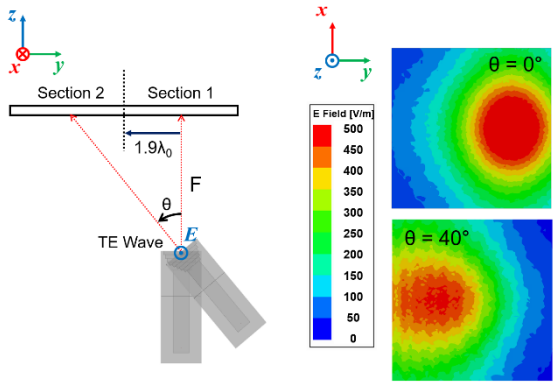

Fig. 4. (a) Rotated feed combined TRIS classified into two sections based on two different radiation centers by beam steering source and (b) electric field intensity of TRIS aperture according to the rotated angle θ.

radiation characteristics since the radiation center to which most of the power from the source is incident is moved by the rotated angle of horn, as shown in Fig. 4(b).

Fig. 5 shows the ideal distribution of a 2-bit quantized unit cell for 0° (broadside) radiation with $\theta = 0°$ horn and $-40°$ radiation with $\theta = 40°$ horn. The deployment of the 2-bit quantized unit cell follows (1), and $\angle$S21 is the required phase for each mainbeam collimation

$$\text{phase}_{\text{2-bit}} = \begin{cases} 270°, & \text{if } 225° \le \angle\text{S21} < 315° \\ 180°, & \text{if } 135° \le \angle\text{S21} < 225° \\ 90°, & \text{if } 45° \le \angle\text{S21} < 135° \\ 0°, & \text{otherwise.} \end{cases} \tag{1}$$

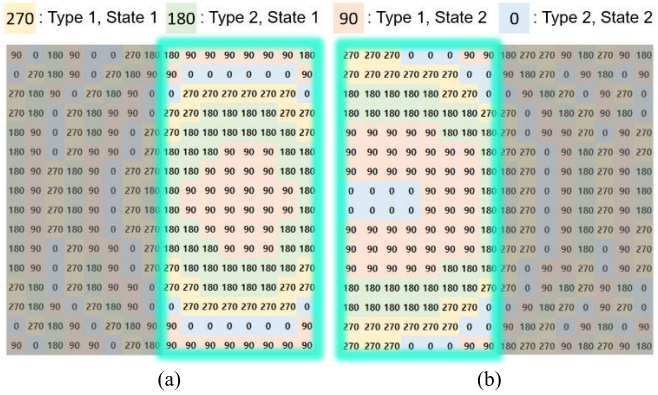

Fig. 5. Ideal distribution of a 2-bit quantized unit cell for (a) 0° (broadside) radiation with $\theta = 0°$ horn and (b) $-40°$ radiation with $\theta = 40°$ horn.

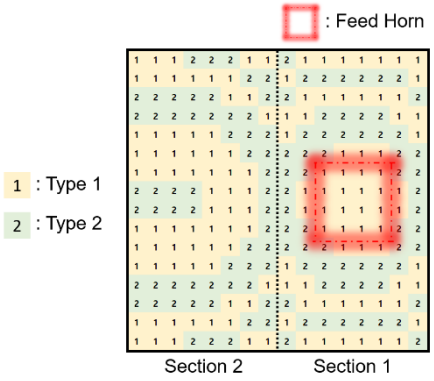

Fig. 6. Optimally deployed 1-bit hybrid units in each section for enhanced 0° (broadside) and $-40°$ collimated beam.

The initial deployment of 1-bit hybrid units is proposed in each section, as shown in Fig. 6, to implement the phase mapping of Fig. 5(a) in Section I and Fig. 5(b) in Section II for optimized gain of 0° and $-40°$ radiation. It should be noted that optimized quasi-2 bit quantization in two mainbeam directions can be implemented with 1-bit hybrid units. The deployment of the 1-bit hybrid unit cell follows

$$\text{phase}_{\text{Type 1}} = \begin{cases} 270°, & \text{if } 180° \le \angle\text{S21} < 360° \\ 90°, & \text{otherwise.} \end{cases}$$
$$\text{phase}_{\text{Type 2}} = \begin{cases} 180°, & \text{if } 90° \le \angle\text{S21} < 270° \\ 0°, & \text{otherwise.} \end{cases} \tag{2}$$

All beamforming cases include optimized directions. However, numerical analysis of array factor (AF) with 1-bit hybrid TRIS is required essentially since the section not including the radiation center also affects the beam collimation. Furthermore, for even array envelope, the analysis of beam scanning capability should be performed except for the optimized directions of 0° and $-40°$.

III. Simulation and Measurement Results

Fig. 7 shows the AF normalized by incident power in the 16 × 16 aperture of a 1-bit hybrid TRIS with a beam steering source and a conventional 1-bit TRIS without a beam steering source. The conventional 1-bit TRIS has a 16 × 16 aperture that is shifted by 1.9 λ_0, which is the same condition as the 1-bit hybrid one, and only type 1 is deployed on the entire aperture. As expected, the gain of 0° and $-40°$ is significantly increased due to 2-bit quantized phase mapping. Also, it is demonstrated that beam collimation except for

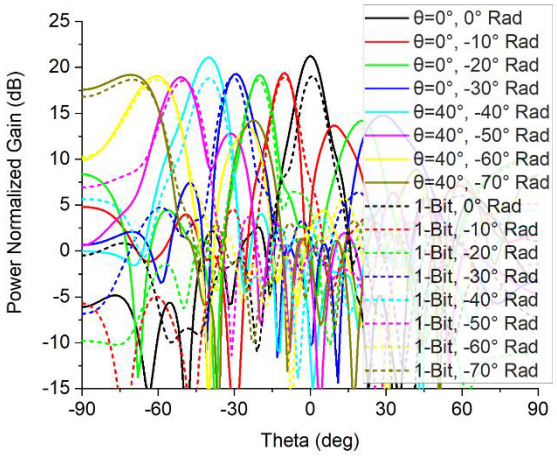

Fig. 7. AF normalized by incident power in 16 × 16 aperture of 1-bit hybrid TRIS with beam steering source and conventional 1 bit TRIS without beam steering source.

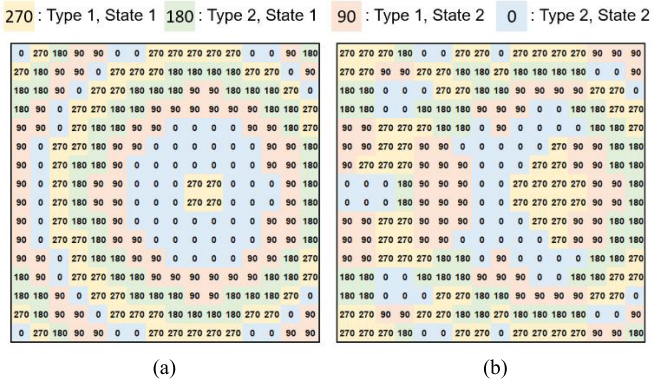

Fig. 8. (a) Ideal 2-bit and (b) quasi 2-bit phase mapping configurations for unoptimized −10° radiation.

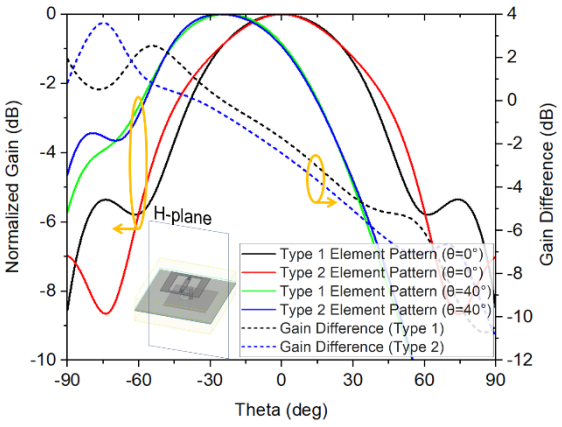

Fig. 9. Normalized element patterns of 1-bit hybrid units according to Floquet incident angle and realized gain difference between 40° and 0° incident angles.

the optimized directions of 0° and −40° is successfully implemented with comparable gain. Fig. 8 shows ideal 2-bit and quasi 2-bit phase mapping configurations for unoptimized −10° radiation. Relatively large minor lobe level, which is particularly prominent in −10° to −30° AF of Fig. 7, is caused by the uneven phase compensation by disparate deployment. Nevertheless, the array envelope is significantly improved for the overall scan angles. However, this AF is a power

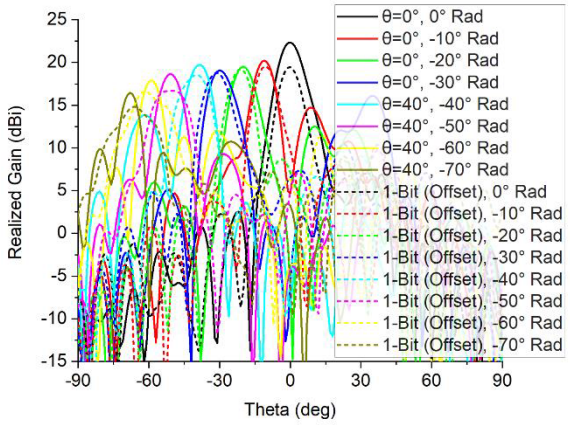

Fig. 10. Simulated radiation patterns of rotated feed combined 1-bit hybrid TRIS and conventional 1-bit one with offset aperture on the H-plane.

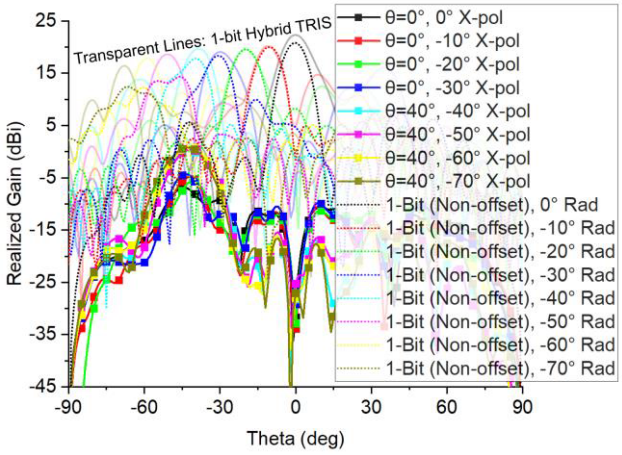

Fig. 11. Simulated co-polarized and cross-polarized radiation patterns of rotated feed combined 1-bit hybrid TRIS and radiation patterns of conventional 1-bit one with nonoffset aperture on the H-plane.

normalized value, in which the insertion loss of the unit cell and the total efficiency of the TRIS aperture are not considered. Therefore, a lower array envelope in −40° to −70° directions can be formed compared to the conventional 1 bit TRIS when the deteriorated transmission characteristics of type 2 and the reduced total efficiency of TRIS aperture combined with $\theta = 40°$ horn are considered. Nevertheless, the additional loss factor for −40° to −70° beam collimation is successfully compensated by the offset of the element patterns of 1-bit hybrid units with rotated horn. Fig. 9 shows the normalized element patterns of 1-bit hybrid units according to Floquet incident angle and the difference in realized gain between $\theta = 40°$ and $\theta = 0°$ incident angles. It should be noted that the peak gain of the Floquet element pattern under the condition of an $\theta = 40°$ incident angle is formed at 30°. That is, the gain difference between $\theta = 40°$ and $\theta = 0°$ shows that the element pattern gain of the offset pattern is greater than that of the nonoffset pattern for angles below −40°. It is found that the gain difference shows a tendency to increase further as the angle decreases from −40°. Fig. 10 shows the simulated radiation patterns of the rotated feed combined 1-bit hybrid TRIS and the conventional 1-bit one without beam steering source on the H-plane. It is demonstrated that the array envelope of 1-bit hybrid TRIS for all beam steering angles is higher than that of conventional 1-bit TRIS. The broadside gain of 1-bit hybrid TRIS is increased by approximately 2.9 dB compared

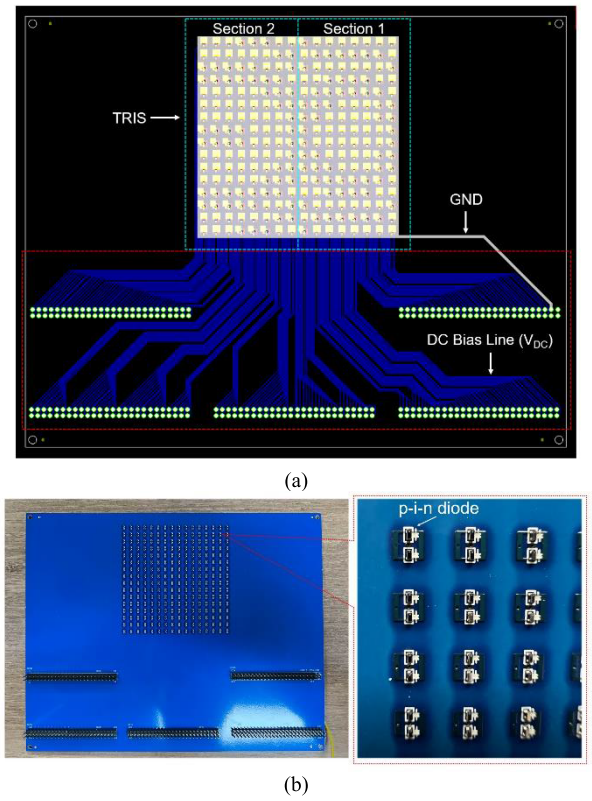

Fig. 12. (a) Design of 1-bit hybrid TRIS with dc bias topology. (b) Fabricated TRIS with mounted p-i-n diodes.

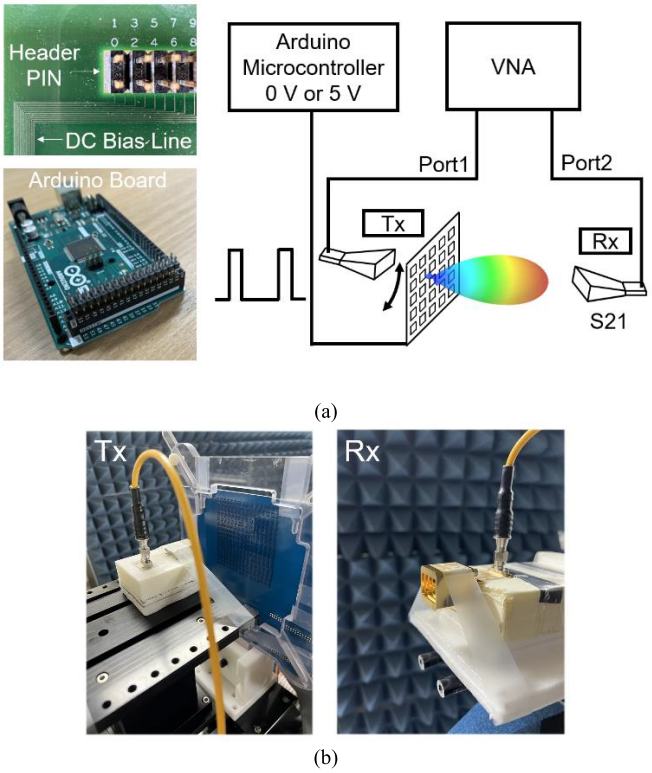

Fig. 13. (a) Schematic of measurement setup of 1 bit hybrid TRIS and (b) measured TRx antennas.

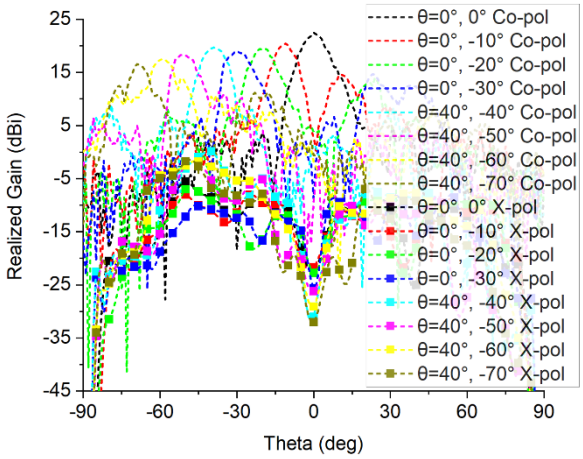

Fig. 14. Measured radiation patterns of rotated feed combined 1 bit hybrid TRIS.

to the conventional 1-bit one. The improved value of 1.2 dB in −40° radiation is lower than that of broadside. As shown in Fig. 9, this is estimated by deteriorated unit cell properties, reduced total efficiency of TRIS aperture, and relatively low gain compensation of offset element pattern in −40°. The enhanced value of each direction from broadside to −70° between two TRIS is 2.9, 0.7, 0.3, 0.3, 1.2, 1.9, 2.3, and 1.6 dB, respectively. Fig. 11 shows the simulated co-polarized and cross-polarized radiation patterns of rotated feed combined 1-bit hybrid TRIS and radiation patterns of conventional 1-bit one with nonoffset aperture on the H-plane. Conventional 1-bit TRIS may not require an offset aperture, so the array envelope is compared for this case additionally. Due to the increase in illumination efficiency, the gain between 0° and −40° slightly increases, but the gain for angles lower than −40° decreases compared to that of the offset aperture. The enhanced value of each direction from broadside to −70° between two TRIS is 2.9, 0, 0, 0.8, 1.9, 4.4, 5.6, and 4 dB, respectively.

Fig. 12 shows the design of a 1-bit hybrid TRIS with dc bias topology and a fabricated one with mounted p-i-n diodes. The dc bias lines connected to each center pad and the dc GND line are in contact with the header pin at the bottom side of the PCB. As shown in Fig. 12(b), 512 diodes are used to control 256 1-bit hybrid units individually. Fig. 13 shows the conceptual drawings of the measurement setup of 1-bit hybrid TRIS and measured TRx antennas. An Arduino microcontroller is used to supply dc bias voltages of 0 or 5 V. Therefore, a potential difference of 2.5 or −2.5 V is realized by applying a voltage of 2.5 V to dc GND. The Rx is a standard horn antenna with a gain of 13 dBi at 28 GHz operating in K-band. Fig. 14 shows the measured radiation patterns of rotated feed combined 1-bit hybrid TRIS. The measured patterns correspond well with the simulation results, and the broadside gain is 22.5 dB, which has an aperture efficiency of 24.4%. The increase of broadside gain of the feed antenna by TRIS is 9.5 dB. Fig. 15 shows the simulated and measured realized gain of 1-bit hybrid TRIS in optimized 0° and −40° directions. Based on the measured values, the 3 dB radiation bandwidths for the two optimized directions are 24.9–30.1 (18.6% in 0°) and 24–30.2 GHz (22.1% in −40°), respectively. Table III shows the comparison between the prior 1-bit TRIS and the proposed 1-bit hybrid one. It should be noted that the proposed 1-bit hybrid TRIS combined with rotated feed source reports higher aperture efficiency compared to that of the previous 1-bit TRIS.

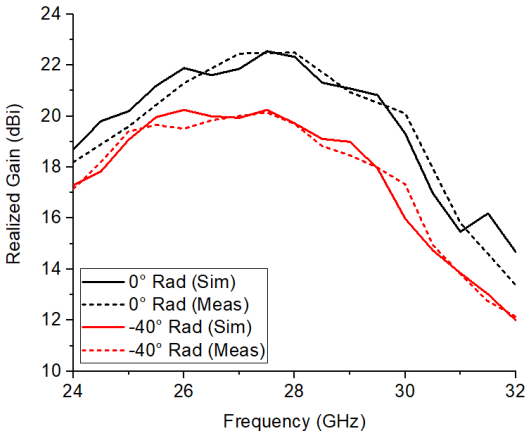

Fig. 15. Simulated and measured realized gain of 1 bit hybrid TRIS in optimized 0° and −40° directions.

TABLE III
COMPARISON BETWEEN PRIOR 1 BIT TRIS AND A PROPOSED 1 BIT HYBRID ONE

Reference	Frequency (GHz)	Scan Range (H-plane)	Aperture Size (λ_0^2)	Measured Gain (dBi)	Aperture Efficiency (%)
[2]	10	-70° to 70°	10×10	22.7	16
[3]	29	-60° to 60°	7×7	19.8	15.9
[5]	17.5	0° to 50°	4.9×4.9	18.3	22.6
[6]	28	-30° to 30°	8.6×8.6	21.4	14.7
[7]	28.4	0° to 50°	5.3×5.3	17	14
This Work	28	-70° to 0°	7.6×7.6	22.5	24.4

IV. CONCLUSION

This communication presented an initial disparate deployment of 1-bit hybrid units of a p-i-n diode-based TRIS combined with a rotated feed source for enhanced array envelope. Two types of 1-bit hybrid units with an equally spaced phase difference of 90° are designed based on delay line topology. The hybrid units are creatively deployed in the TRIS aperture classified into two sections by the radiation centers of the rotated feed source to realize an improved array envelope in all directions, even in radiation directions other than the optimized ones. The proposed 1-bit hybrid TRIS yields an aperture efficiency of 24.4%. It will be possible to attain improved beamforming performance with a larger area in TRIS applications, wherein the reduction of spillover efficiency by the beam steering source can be minimized.

REFERENCES

[1] G. S. Shin et al., "Low insertion loss, compact 4-bit phase shifter in 65 nm CMOS for 5G applications," *IEEE Microw. Wireless Compon. Lett.*, vol. 26, no. 1, pp. 37–39, Jan. 2016, doi: 10.1109/LMWC.2015.2505624.

[2] A. Clemente, L. Dussopt, R. Sauleau, P. Potier, and P. Pouliguen, "Wideband 400-element electronically reconfigurable transmitarray in X band," *IEEE Trans. Antennas Propag.*, vol. 61, no. 10, pp. 5017–5027, Oct. 2013, doi: 10.1109/TAP.2013.2271493.

[3] F. Diaby, A. Clemente, R. Sauleau, K. T. Pham, and L. Dussopt, "2 bit reconfigurable unit-cell and electronically steerable transmitarray at *Ka*-band," *IEEE Trans. Antennas Propag.*, vol. 68, no. 6, pp. 5003–5008, Jun. 2020, doi: 10.1109/TAP.2019.2955655.

[4] L. D. Palma, A. Clemente, L. Dussopt, R. Sauleau, P. Potier, and P. Pouliguen, "Circularly-polarized reconfigurable transmitarray in Ka-band with beam scanning and polarization switching capabilities," *IEEE Trans. Antennas Propag.*, vol. 65, no. 2, pp. 529–540, Feb. 2017, doi: 10.1109/TAP.2016.2633067.

[5] Y. Wang, S. Xu, F. Yang, and D. H. Werner, "1 bit dual-linear polarized reconfigurable transmitarray antenna using asymmetric dipole elements with parasitic bypass dipoles," *IEEE Trans. Antennas Propag.*, vol. 69, no. 2, pp. 1188–1192, Feb. 2021, doi: 10.1109/TAP.2020.3005713.

[6] Y. Wang, S. Xu, F. Yang, and M. Li, "A novel 1-bit wide-angle beam scanning reconfigurable transmitarray antenna using an equivalent magnetic dipole element," *IEEE Trans. Antennas Propag.*, vol. 68, no. 7, pp. 5691–5695, Jul. 2020, doi: 10.1109/TAP.2020.2964954.

[7] M. Wang, S. Xu, F. Yang, and M. Li, "Design and measurement of a 1-bit reconfigurable transmitarray with subwavelength H-shaped coupling slot elements," *IEEE Trans. Antennas Propag.*, vol. 67, no. 5, pp. 3500–3504, May 2019, doi: 10.1109/TAP.2019.2902676.

[8] A. Clemente, L. Dussopt, R. Sauleau, P. Potier, and P. Pouliguen, "1-bit reconfigurable unit cell based on PIN diodes for transmit-array applications in *X*-band," *IEEE Trans. Antennas Propag.*, vol. 60, no. 5, pp. 2260–2269, May 2012, doi: 10.1109/TAP.2012.2189716.

[9] L. Di Palma, A. Clemente, L. Dussopt, R. Sauleau, P. Potier, and P. Pouliguen, "1-bit reconfigurable unit cell for Ka-band transmitarrays," *IEEE Antennas Wireless Propag. Lett*, vol. 15, pp. 560–563, 2016, doi: 10.1109/LAWP.2015.2458179.

[10] X. Bai et al., "Dynamic millimeter-wave OAM beam generation through programmable metasurface," *Nanophotonics*, vol. 11, no. 7, pp. 1389–1399, Apr. 2022.

[11] B. Wu, A. Sutinjo, M. E. Potter, and M. Okoniewski, "On the selection of the number of bits to control a dynamic digital MEMS reflectarray," *IEEE Antennas Wireless Propag. Lett.*, vol. 7, pp. 183–186, 2008, doi: 10.1109/LAWP.2008.920908.

[12] A. Yu, F. Yang, A. Z. Elsherbeni, J. Huang, and Y. Rahmat-Samii, "Aperture efficiency analysis of reflectarray antennas," *Microw. Opt. Technol. Lett.*, vol. 52, pp. 364–372, Sep. 2010.

[13] Q. Chen et al., "Electronically reconfigurable unit cell for transmit-reflect-arrays in the X-band," *Opt. Exp.*, vol. 29, no. 2, pp. 1470–1480, Jan. 2021.

[14] B. D. Nguyen and C. Pichot, "Unit-cell loaded with PIN diodes for 1-bit linearly polarized reconfigurable transmitarrays," *IEEE Antennas Wireless Propag. Lett.*, vol. 18, no. 1, pp. 98–102, Jan. 2019, doi: 10.1109/LAWP.2018.2881555.

[15] W. Pan, C. Huang, X. Ma, B. Jiang, and X. Luo, "A dual linearly polarized transmitarray element with 1-bit phase resolution in X-band," *IEEE Antennas Wireless Propag. Lett.*, vol. 14, pp. 167–170, 2015, doi: 10.1109/LAWP.2014.2358267.

[16] M. Wang, S. Xu, F. Yang, N. Hu, W. Xie, and Z. Chen, "A novel 1-bit reconfigurable transmitarray antenna using a C-shaped probe-fed patch element with broadened bandwidth and enhanced efficiency," *IEEE Access*, vol. 8, pp. 120124–120133, 2020, doi: 10.1109/ACCESS.2020.3004435.

[17] H. Kim, J. Kim, and J. Oh, "Communication a novel systematic design of high-aperture-efficiency 2D beam-scanning liquid-crystal embedded reflectarray antenna for 6G FR3 and radar applications," *IEEE Trans. Antennas Propag.*, vol. 70, no. 11, pp. 11194–11198, Nov. 2022, doi: 10.1109/TAP.2022.3209178.

[18] J. Lee, H. Kim, and J. Oh, "Large-aperture metamaterial lens antenna for multi-layer MIMO transmission for 6G," *IEEE Access*, vol. 10, pp. 20486–20495, 2022, doi: 10.1109/ACCESS.2022.3150037.

[19] H. Kim, J. Kim, and J. Oh, "Liquid-crystal-based X-band reactively loaded reflectarray unit cell to reduce reflection loss," *IEEE Antennas Wireless Propag. Lett.*, vol. 20, no. 10, pp. 1898–1902, Oct. 2021, doi: 10.1109/LAWP.2021.3099818.

[20] B. Rana, I.-G. Lee, and I.-P. Hong, "Experimental characterization of 2 × 2 electronically reconfigurable 1-bit unit cells for a beamforming transmitarray at X band," *J. Electromagn. Eng. Sci.*, vol. 21, no. 2, pp. 153–160, Apr. 2021.